Published in final edited form as:

Nat Nanotechnol. 2020 August ; 15(8): 716–723. doi:10.1038/s41565-020-0719-0.

Role of nanoscale antigen organization on B-cell activation probed using DNA origami

Rémi Veneziano[1,†,#], **Tyson J. Moyer**[2,†], **Matthew B. Stone**[1,†], **Eike-Christian Wamhoff**[1], **Benjamin J. Read**[2], **Sayak Mukherjee**[3], **Tyson R. Shepherd**[1], **Jayajit Das**[3], **William R. Schief**[4,5,6,7], **Darrell J. Irvine**[1,2,3,6,7,8,*], **Mark Bathe**[1,*]

[1]Massachusetts Institute of Technology, Department of Biological Engineering, Cambridge, Massachusetts 02139, United States

[2]Massachusetts Institute of Technology, Koch Institute for Integrative Cancer Research, Cambridge, Massachusetts 02139, United States

[3]The Ohio State University, Battelle Center for Mathematical Medicine, The Research Institute at Nationwide Children's Hospital, Department of Pediatrics, Columbus, Ohio 43205, United States

[4]Center for HIV/AIDS Vaccine Immunology and Immunogen Discovery, The Scripps Research Institute, La Jolla, California 92037, United States

[5]International AIDS Vaccine Initiative Neutralizing Antibody Center, The Scripps Research Institute, La Jolla, California 92037, United States

[6]Dept. of Immunology and Microbial Science, The Scripps Research Institute, La Jolla, CA 92037 United States

[*]Address correspondence to mark.bathe@mit.edu and djirvine@mit.edu.

[#]Present address: George Mason University, Volgenau School of Engineering, Department of Bioengineering, Fairfax, VA 22030-4422, USA

[†]These authors contributed equally

Author Contributions

R.V. designed the different DNA-NPs and performed the folding and characterization of the DNA-NPs, the conjugations with different antigens, and their fluorescence quantification measurements, and analyzed the data. T.J.M. performed the antigen modification with PNA and fluorescent dye, the B cell calcium flux assay, the flow cytometry, and analyzed the data. M.B.S. performed the confocal microscopy imaging, the image analysis, and analyzed the data. E.W. performed additional DNA-NPs synthesis, modification with antigens and characterization. T.R.S. performed the TEM characterization. B.J.R. performed additional antigen modification with PNA, B cell calcium flux, and data analysis. S.M. and J.D. developed the in silico model. S.M. developed computer codes and S.M. and J.D. simulated the model and analyzed the data. W.R.S. designed the immunogens. M.B. and D.J.I. designed and supervised the study and interpreted the results. R.V., T.J.M., M.B.S., J.D., D.J.I., and M.B. wrote the manuscript. All authors commented on and edited the manuscript.

Competing Interests Statement

The authors declare no competing financial and/or non-financial interests.

Data availability

The raw data that support the plots within this paper are available from the authors upon reasonable request.

Code availability

Computer code is available from Github at: https://github.com/jayajitdas/bcr-signaling-model

Additional information

Supplementary information is available in the online version of the paper. Reprints and permission information is available online at www.nature.com/reprints. Correspondence and requests for materials should be addressed to MB and DJI.

[7]Ragon Institute of Massachusetts General Hospital, Massachusetts Institute of Technology and Harvard University, Cambridge, Massachusetts 02139 United States

[8]Massachusetts Institute of Technology, Department of Materials Science and Engineering, Cambridge, Massachusetts 02139, United States

[9]Howard Hughes Medical Institute, Chevy Chase, Maryland 20815, United States

Abstract

Vaccine efficacy can be increased by arraying immunogens in multivalent form on virus-like nanoparticles to enhance B cell activation. However, the effects of antigen copy number, spacing, and affinity, as well as the dimensionality and rigidity of scaffold presentation on B cell activation remain poorly understood. Here, we displayed the clinical vaccine immunogen eOD-GT8, an engineered outer domain of the HIV-1 glycoprotein-120, on DNA origami nanoparticles to systematically interrogate the impact of these nanoscale parameters on B cell activation in vitro. We found that B cell signalling is maximized by as few as five antigens maximally spaced on the surface of a 40 nm viral-like nanoparticle. Increasing antigen spacing up to ~25–30 nm monotonically increases B cell receptor activation. Moreover, scaffold rigidity is essential for robust B cell triggering. These results reveal molecular vaccine design principles that may be used to drive functional B cell responses.

Efficient activation of antigen-specific B cells is a central goal in the design of new vaccines. One well established strategy to enhance B cell activation employs multivalent presentation of immunogens[1]. Antigen multimers, antigen-conjugated polymers, and virus-like nanoparticles (NPs) displaying immunogens at high density have all been shown to strongly initiate early B cell signaling[2–6]. Antigen multimerization enables low affinity B cells to be fully activated[7,8], which may be particularly important for approaches such as lineage-guided or germline-targeting (GT) vaccines that aim to activate specific rare, low-affinity target B cell populations[9–13]. However, the independent roles of antigen spatial arrangement and additional design parameters (including antigen copy number, affinity, and rigidity and dimensionality of scaffold presentation) in triggering B cells and initiating robust BCR signaling remain poorly understood. To date, studies exploring the effect of antigen organization on B cell triggering have generally employed protein, polymer, or particle scaffolds that only allowed limited variation of the preceding design parameters, or provided only statistical control over the numbers and locations of antigens[2,3,14–16]. In order to independently probe the relative roles of immunogen valency and spacing on IgM-BCR activation, here we used scaffolded DNA origami NPs[17–19] to display discrete antigen copy numbers with controlled inter-antigen spacings on the scale of an individual virus-like NP. As a clinically relevant model antigen, we focused on the GT engineered outer domain (eOD) of the HIV-1 envelope glycoprotein antigen gp120, termed eOD-GT8[20]. This antigen was designed to bind with high affinity to the inferred germline precursor of the VRC01 CD4 binding site-specific HIV broadly neutralizing antibody (glVRC01), and thereby activate a collection of human naïve B cells expressing so-called VRC01-class IgM-BCRs[13,21,22]. eOD-GT8 activates both cognate glVRC01 IgM-BCR-expressing cell lines and murine BCR-transgenic primary B cells (K_D ~ 30 pM), but only when presented to B cells in multivalent form[8,21]. Schief and colleagues showed that multimerization of 60

copies of eOD-GT8 via fusion to the self-assembling bacterial protein lumazine synthase formed an isotropic ~30 nm diameter NP (eOD-60mer) that elicited robust B cell activation *in vitro* and *in vivo*[12,20,21]. Here, to interrogate the relative roles of antigen spacing, copy number, and dimensionality and rigidity of scaffold presentation on B cell activation *in vitro*, we used DNA origami to spatially present eOD-GT8. Key findings were recapitulated with a lower affinity eOD-GT variant and model peptide antigens recognized by primary murine B cells. We also interpret our results in the broader context of a mechanistic, molecular-level reaction-diffusion model of membrane proximal IgM-BCR signaling kinetics.

To systematically probe the independent roles of antigen copy number versus spacing on B cell triggering, we focused on two structured DNA-NP[17,18] variants: A 3D icosahedral NP[18] with a ~40 nm diameter size that is comparable to the eOD-60mer and a 1D rigid-rod six-helix bundle (6HB) of ~80 nm maximal dimension (Fig. 1a and Supplementary Figs. 1 and 2). eOD-GT8 antigens were site-specifically coupled to these nanostructures through hybridization to free single-stranded DNA (ssDNA) overhang strands displayed from the origami at specific, spatially programmed locations (Supplementary fig. 3). Using this approach, we were able to present the antigen in copy numbers varying from 1 to 60 in variable nanoscale spatial organizations, enabling independent control over antigen stoichiometry, inter-antigen distance, as well as the spatial dimensionality of antigen presentation (Fig. 1b).

As comparative controls to test the impact of DNA-NP scaffold rigidity on IgM-BCR activation, we prepared dimer constructs presented on flexible ssDNA or polyethylene glycol (PEG) polymer linkers of varying lengths (Supplementary Table 1). To generalize our results to other antigens and immunogen-presentation scaffolds, we also examined a lower affinity variant of eOD-GT8, as well as distinct peptide model antigens, which we displayed using either liposomes (Lipos) or a pentagonal bipyramid origami NP (See Supplementary Materials).

Negative stain transmission electron microscopy (TEM) imaging and agarose gel electrophoresis of the 6HB and icosahedral DNA-NP constructs confirmed their geometry, monodispersity, and structural rigidity, consistent with previous work[18] (Fig. 2a and Supplementary Figs. 4–7). Short, outward-facing ssDNA overhangs were used at the 3’ ends of select DNA-NP staple strands to anchor individual eOD-GT8 monomers (Supplementary Fig. 3) via hybridization to a complementary peptide nucleic acid (PNA) tag site-specifically conjugated to the antigen (Supplementary Figs. 8–10). PNA strands are synthetic polymers that mimic nucleic acids in their hybridization affinity and specificity via Watson-Crick base-pairing, yet their uncharged peptide backbone that replaces the phosphate backbone of DNA results in a higher binding affinity with DNA compared with DNA:DNA hybridization[23]. eOD-GT8-PNA monomers were purified and added to pre-folded and purified DNA-NPs to allow for complete hybridization prior to purification and application to B cells *in vitro*. Antigen-coupled NPs showed expected shifts in gel electrophoresis (Fig. 2b), while fluorimetry (using a fluorescent version of the PNA-eOD-GT8 labeled with AlexaFluor647) and tryptophan fluorescence measurements confirmed efficient and stable complexation of eOD-GT8-PNA to DNA-NPs with quantitatively controlled stoichiometries varying from 2 to 60 (Fig. 2b, Supplementary Figs. 11–13).

Effect of immunogen organization on B cell triggering

We first analyzed the impact of eOD-GT8 valency on B cell response using the ~40 nm diameter icosahedral DNA-NP bearing zero to ten copies of eOD-GT8 monomers distributed equidistantly from one another over the surface of the NP ([0–10]-mer, Supplementary Fig. 14 and Supplementary Table 2). As a readout of IgM-BCR triggering, we focused on dynamic measurements of intracellular calcium signaling as a critical signature of full IgM-BCR activation[24]. Human Ramos B cells stably expressing the eOD-GT8 antigen's cognate germline VRC01 IgM receptor were incubated with DNA-NPs equivalent to 0.5 nM or 5 nM total eOD-GT8, or the same eOD-equivalent concentration of eOD-GT8–60mer protein NPs, with B cell responses recorded spectroscopically using a fluorescent intracellular calcium indicator dye. As expected[8,21], antigen-free DNA-NPs or NPs bearing a single copy of eOD failed to activate B cells at either antigen concentration. In contrast, NPs bearing two or more copies of eOD-GT8 triggered monotonically increasing cellular responses with increasing antigen valency (Fig. 2c and d). Intriguingly, at both antigen concentrations, signaling plateaued with 5-mer or higher valency DNA-NPs, at a level indistinguishable from the eOD-GT8–60mer. Moreover, increasing the valency of the DNA icosahedron to 30 or 60 copies of eOD-GT8 had no further effect on increasing cellular response (Supplementary Fig. 15). Because the affinity of eOD-GT8 for glVRC01 is high, with a K_D ~ 30 pM[21], we also tested the same icosahedral DNA-NP functionalized with a lower-affinity variant, eOD-GT5 (K_D ~0.5μM[8,21]) (Supplementary Fig. 16). As observed with eOD-GT8, the five and ten copy number icosahedral NPs exhibited a similar plateau in signaling when conjugated with eOD-GT5. Interestingly, however, even at an eOD-GT5 concentration of 25 nM, maximum activation remained lower than that observed with the eOD-GT8–60-mer at the considerably lower immunogen concentration of 2 nM.

Next we sought to define the impact of antigen spacing on IgM-BCR triggering. Previous studies have shown that inter-antigen separations impact receptor signaling for both Fc receptor engaging IgE[25] and the T cell receptor[26], and that nanoscale organization of the BCR crucially impacts receptor activation[5,27–30]. To evaluate antigen spacing in the absence of potentially confounding 3D geometric variation, we turned to a 1D rigid DNA origami rod made from a simple 6HB to first present antigen dimers using variable, fixed inter-antigen spacings (Supplementary Figs. 2 and 3). Calcium signaling in responding B cells was triggered at the closest dimer spacing tested of ~7 nm (+/− 3 nm linker size), and surprisingly subsequently increased monotonically with increasing antigen spacing at fixed total antigen concentration (Fig. 3a). Calcium responses appeared to plateau at an antigen spacing of ~25–30 nm, yet remained elevated at a spacing of ~80 nm, despite the fact that this latter spacing would preclude binding of the rod-like antigen dimer to two closely spaced IgM-BCRs, or to a single IgM-BCR because this distance is well beyond the spatial tolerance anticipated for a single IgM-BCR[31]. While in this study we did not test dimer distances larger than 80 nm, we confirmed that enhanced triggering by widely-spaced dimers was not due to differences in overall IgM-BCR engagement with the nanostructures, because flow cytometry analysis of fluorescent 6HB association with Ramos cells showed essentially identical binding of 7 nm-spaced eOD dimers and 28 nm-spaced dimers to B cells after a 30-minute incubation with the constructs in comparison with the increase level

of binding observed for a higher number of antigens presented by the construct Ico-30x (Fig. 3b and Supplementary Fig. 17).

To test the role of fixed inter-antigen spacing imparted by DNA-NP scaffold rigidity on IgM-BCR triggering by dimeric antigens, we compared calcium signaling induced by rigid DNA origami rods to eOD-GT8 dimers presented using flexible ssDNA or PEG linkers of variable contour lengths (Supplementary Table 1). These flexible polymer constructs presenting eOD-GT8 dimers elicited substantially reduced B cell signaling compared with their rigid DNA-NP counterparts, indicating the importance of both inter-antigen distance and also rigidity of the structural scaffold used to present antigens themselves for inducing robust B cell response (Fig. 3c).

To further investigate the relative roles of inter-antigen spacing and dimensionality of presentation on B cell response, we programmed different clusters of five eOD-GT8 antigens on one face of the icosahedral DNA-NP using distinct inter-antigen distances of ~3 to 22 nm (or a maximum inter-antigen spacing of 36 nm), and we also varied the DNA origami NP scaffold geometry itself (Fig. 4a and b, Supplementary figs. 18–20). We found that increasing inter-antigen distances on the DNA icosahedron also led to a monotonic increase in cellular response, similar to that observed with the dimer presented on a rigid-rod origami (Figure 3). For inter-antigen distances greater than ~22 nm, cellular responses also appeared to plateau (Supplementary fig. 18), although considerably larger origami objects would be needed to rigorously establish cellular behavior beyond this upper limit observed. Using the rigid rod to alternatively display 5 antigens in a linear manner with similar minimum inter-antigen distances showed that decreasing inter-antigen distance also yielded decreasing cellular response, consistent with our observations with the 6HB dimer DNA-NP (Supplementary Fig. 18). However, for the smaller minimal inter-antigen distances of 7 and 11 nm, linear antigen display yielded a relatively higher response than the quasi-planar organization of antigens (Supplementary fig. 18), likely due to its larger mean or maximal inter-antigen spacings: For example, the 6HB-5x-11 nm mean and maximal spacings are 22 nm and 44 nm (Supplementary fig. 19).

To test the potential role of 3D DNA-NP geometry on IgM-BCR triggering, we also designed a disk-like pentagonal bipyramid to compare cellular activation with the icosahedron. At an antigen copy number of 10, we observed similarly robust B-cell activation, comparable with the icosahedron and the eOD-GT8–60mer reference particle (Supplementary Fig. 20). To test the generality of our DNA-NP platform for presentation of other antigens and to evaluate whether similar NPs could activate naïve primary B cells, we hybridized the pentagonal bipyramid with short linear peptide antigens, which are recognized by murine 3–83 IgM-BCR-transgenic B cells.[32] 45 copies of medium- (p31, K_D = 15.3 nM) or low-affinity (p5, K_D = 1 uM) peptide antigens were conjugated, and IgM-BCR triggering was compared with presentation Lipos, a common synthetic vaccine platform. While activation levels were comparable between all three constructs, IgM-BCR triggering appeared to be slightly delayed in the case of the Lipos, despite their considerably higher total copy number of immunogens, their similar mean inter-antigen spacing (~7 versus 11 nm for the DNA-NP and Lipo, respectively), and their larger overall particle size (Supplementary fig. 21). This observation further supports the importance of scaffold

rigidity and fixed inter-antigen spacing for efficient B cell triggering, even for low affinity antigens.

Imaging of early events in DNA-NP binding to B cells

To probe the mechanism of B cell activation, we examined three distinct DNA-NP constructs using fluorescence imaging: two 6HB dimers with inter-antigen spacings of 7 and 28 nm that respectively triggered low and high B cell activation, and one DNA icosahedral NP presenting 30 copies of eOD-GT8 that triggered robust B cell activation. Fluorescently labeled eOD-GT8-presenting DNA-NPs were added to Ramos cells at identical total eOD-GT8 concentrations and spatially correlated with fluorescently labeled IgM-BCR on the cell surface prior to internalization (Fig. 5a and Supplementary Figs. 22–24). As anticipated, DNA-NP binding was strongly correlated with VRC01 IgM expression, whereas cells lacking IgM expression failed to bind the eOD-GT8-bearing particles (Fig. 5b and Supplementary Figs. 22–24). For all DNA-NP constructs examined, antibody staining of phosphorylated Syk kinase (pSyk) revealed a sharp increase in pSyk phosphorylation after only 1 minute of DNA-NP or eOD-GT8–60mer addition. Moreover, dimers of eOD-GT8 separated by short distances of only 7 nm (6HB-2x-7nm) resulted in significantly lower pSyk accumulation compared with dimers separated by larger distances of 28 nm (6HB-2x-28 nm) or icosahedral NPs bearing 30 copies of eOD-GT8 (Ico-30x)(Fig. 5c). Characterization of the internalization of eOD using phalloidin to stain filamentous actin in the actin-rich cellular cortex indicated greater internalization of the icosahedral 30-mer NP compared with its 6HB-2x-7 nm and 6HB-2x-28 nm counterparts (Fig. 5d). Taken together, these results corroborated both the levels of cellular activation observed for these three DNA-NP constructs, and affirm that the previously observed calcium responses were acting through the IgM-BCR-mediated activation pathway that includes pSyk phosphorylation and downstream NP internalization.

Modeling of early BCR signaling following B cell triggering by DNA-NPs

Consistent with previous studies and models of B cell triggering, we observed that nanometer-scale distances between immunogens and their valency[2,3,6] are both crucial determinants of IgM-BCR activation and cellular response[27–30,33]. However, our results also point clearly to the importance of scaffold rigidity to maintain inter-antigen separations for optimal IgM-BCR activation. Interestingly, we observed a monotonic increase in cellular activation in both linear and quasi-planar spatial antigen presentations up to a spacing of approximately ~25–30 nm (Supplementary fig. 18). In addition, our results showed sustained, efficient signaling induction for an 80 nm dimer (Fig. 3a), suggesting that antigen engagement of non-local, distal B cell receptors can also drive the initiation of signaling in response to antigen binding. While these non-local interactions may stem from a variety of sources that would require sophisticated single-molecule imaging and molecular perturbation analyses to dissect, two discrete possibilities include signaling cooperativity between the antigen receptor and slowly evolving structural elements within the B cell membrane[34] and the actin cortex[35], which could facilitate communication of receptor binding over such large distances[28], or spatially-mediated positive feedback between signaling components downstream of IgM-BCR, as explored in previous work[36].

To explore the latter hypothesis theoretically, we applied an *in silico* coarse-grained reaction-diffusion model to our system that was previously used to describe BCR signaling (Supplementary Text 1 and Supplementary Figs. 25 and 26)[36]. The model describes early time membrane proximal IgM-BCR signaling initiated by IgM-BCR-antigen binding of glVRC01 IgM to eOD-GT8 antigens followed by ITAM phosphorylation mediated by reaction-diffusion of Lyn and Syk, where antigen unbinding events are neglected due to the slow off-rate of this antigen/receptor pair (k_{off} < 5.05E-5 s^{-1})[20]. This model is agnostic toward competing mechanisms previously proposed for BCR triggering[37], namely, disintegration of auto-inhibited BCR multimers upon antigen binding into smaller active BCR clusters[27], formation of BCR clusters due to conformational change in antigen binding BCRs[30,38], or actin-mediated restriction of BCR mobility limiting ITAM phosphorylation[33]. In the model, monomeric IgM-BCRs engage with each antigen on the origami, where IgM-BCR clusters are formed at the nanoscale (~30nm) upon binding (Supplementary Text 1), as justified by several experiments[29,37] including super-resolution microscopy[29,39], as well as our own data (Supplementary Figs. 23 and 24). While our model does not propose any specific mechanism for this clustering, it explores the consequence of such spatial clustering on B cell activation through IgM-BCR. Our results show (Supplementary Text 1 and Supplementary Fig. 25) that antigens separated by less than 30 nm limit the total amount of IgM-BCRs recruited to each antigen due to steric exclusion. Thus, as inter-antigen separation increases, IgM-BCR signaling increases until the IgM-BCR clusters are no longer overlapping, resulting in a signaling plateau (Supplementary Fig. 26). A similar plateau was observed theoretically for lower affinity antigen, albeit at a lower level of activation, as observed experimentally for the lower affinity antigen variant eOD-GT5 (Supplementary Fig. 16 and Supplementary text 1 and Supplementary Fig. 25 and 26). And while a similar monotonic increase in signaling was observed *in silico* for increasing minimum inter-antigen spacing in a planar, 2D pentameric spatial organization, saturation in cellular activation was observed experimentally in the linear pentameric construct at smaller minimum inter-antigen spacings than in the model. Thus, while this model offers a potential mechanism by which monotonic increase in B cell activation arises as inter-antigen spacing increases, additional factors must limit cellular activation once any inter-antigen distances of ~25–30nm are attained.

Conclusions

In summary, using DNA origami as a platform for controlling the spatial presentation of eODGT8 antigens, we identify here several design criteria maximizing early B cell triggering, including valency of 5 or more antigens, nearest neighbor spacings of ~25–30 nm or greater, and use of a rigid scaffold for antigen display. Additional modeling studies may be combined in the future with advanced super-resolution and single-molecule imaging to explore alternative, competing hypotheses such as the presence of actin “corrals” that may also contribute to explaining these experimental observations. In addition, the relative roles of monomeric versus dimeric binding to individual IgM-BCRs based on the spatial tolerance of IgM, which is not captured in our model, would also be interesting to explore with single-particle-based, stochastic models in future work[31]. Finally, affinity is also an important determination of BCR responses[32,40], where we reiterate that the affinity between germ-line

VRCO1 and eOD-GT8 is in the sub-nanomolar range, placing this system in the regime of mature IgM-BCR antigen affinities, rather than naïve affinities. In the case of lower affinity interactions, as explored for the eOD-GT5 and model peptide antigen, higher multivalency might play a more prominent role in B cell activation. Indeed, it has been suggested that the low number of Env viral spikes displayed on the viral surface of HIV may help it to evade detection by the immune system[41]. Notwithstanding, for the purpose of rational design of molecular vaccines for robust triggering of B cell responses, here DNA origami offered crucial insight into the spatial relationships between immunogens, which may be generalized to other viral pathogens such as SARS-CoV-2 and Zika, and offered important foundations for the rational design of protein-based and other vaccine platforms[42].

Methods

- Chemicals and kits

Magnesium chloride, TRIS acetate EDTA (TAE) buffer, TRIS-base, sodium chloride, Phosphate Buffer Saline, ethidium Bromide solution (10 mg/mL), Pluronic F-127 (#540025–50ML) and Amicon ultra 0.5 centrifugal filter (#UFC5003) were provided by Sigma-Aldrich. Nuclease free water was purchased from Integrated DNA Technologies, Inc. (IDT). The DNTPs mix (#N0447S), the DNA ladder (Quick-Load® Purple 2-Log DNA ladder 0.1–10 kb, #N0550S) were provided by New England Biolabs (NEB), The polymerase enzyme (Accustart Taq DNA polymerase HiFi, #95085–05K) was provided by Quanta Biosciences. Low melt agarose was purchased from IBI Scientific (#IB70058) and the agarose from Seakem, Inc. G-capsule for electroelution (#786–001) was purchased from G-Biosciences and Freeze ‘N Squeeze DNA gel extraction columns by Bio-rad, Inc. (#732–6165). The Zymoclean Gel DNA recovery kit (#D4008) was purchased from Zymo Research, Inc. The SybrSafe DNA staining reagent was provided by Thermo Fisher Scientific, Inc. PEG3500 (#A4010–1/MAL-PEG3500-MAL) and PEG2000 (#A4010–1/MAL-PEG2000-MAL) bismaleimide were purchased from JenKem Technology.

- Oligonucleotides and DNA templates

All oligonucleotides used for asymmetric PCR (aPCR) amplification of the template and for folding the various scaffolded DNA origami nanoparticles (NPs) were purchased from IDT. The circular plasmid DNA scaffold M13mp18 used for amplification of the short scaffolds with aPCR (Supplementary sequences are provided in the supplementary Table 10–17) was acquired from NEB (#N4040S).

- Antigens and cell lines

The eOD antigen with a 6xHis tag and N-terminal cysteine was prepared as previously described[20]. Plasmids were transiently transfected into Expi293 cells (ThermoFisher Scientific, not authenticated). After 5 days, cell culture supernatants were collected and protein was purified in an ÄKTA pure chromatography system using HiTrap HP Ni sepharose affinity column, followed by size exclusion chromatography using Superdex 75 Increase 10/300 GL column (GE Healthcare Life Sciences). Endotoxin levels in purified protein was measured using Endosafe Nexgen-PTS system (Charles River) and assured to be < 5EU/mg protein. PNA conjugated peptide antigens p31 (HDWRSGFGGFQHLCC-O-

Linker-cagtccagt-K(AF-647)) and p5 (SGSVTYLPTPEWALQSGS-O-Linker-cagtccagt-K(AF-647)) were purchased from PNA Bio. Ramos B cells stably expressing VRC01 germline IgM B cell receptor were provided by Dr. Daniel Lingwood (Ragon Institute of MGH, MIT and Harvard)[43,44]. As described previously, VRC01 germline cells were generated by stable lentiviral transduction of surface IgM-negative Ramos B cells and IgM-BCR-expressing cells were sorted by flow cytometry. Antigen-specific receptor expression levels after transduction were characterized previously and found to be ~12,000 per cell[44]. Functional expression of germline VRC01 was confirmed by flow cytometry analysis of labeled eOD probes binding to the VRC01 Ramos cells. Both Expi293 and germline VRC01-expressing Ramos B cells tested negative for mycoplasma.

- **ssDNA scaffold synthesis**

The ssDNA scaffolds used to fold the DNA six helix bundle (6-HB) and the DNA icosahedron NPs were produced using the previously described procedure asymmetric PCR[18,45]. Briefly, two specific primers sets were used to amplify the ssDNA fragments (Supplementary Table 3) using Quanta Accustart HiFi DNA polymerase. The aPCR mix was prepared at a final volume of 50 μL with the specific polymerase buffer complemented with 2 mM magnesium chloride, 200 μM dNTPs, 1μM forward primer, 20 nM reverse primer, 25 ng M13mp18 template, and 1 unit of Quanta Accustart HiFi polymerase. The amplification protocol used was: 94°C for 1 min for initial denaturation followed by 35 cycles of 94°C held for 20 sec; 56°C held for 30 sec; 68°C held for 1 min per kb for amplification. Following amplification, the aPCR mix was run on a 1% low-melt agarose gel prestained with Ethidium Bromide (EtBr). The resulting ssDNA product was then extracted using the Zymoclean gel DNA recovery kit. The custom circular DNA scaffold phPB84 used for the pentagonal bipyramid DNA-NP was prepared as previously published[46]. Purified ssDNA concentration was measured using a NanoDrop 2000 (Thermo Scientific).

- **DNA-NP folding**

DNA-NPs (icosahedron, pentagonal bipyramid, and 6-HB) with or without overhangs were self-assembled using a one-pot reaction and annealing as described previously[17,18]. Briefly, 20–40 nM of scaffold was mixed with an excess of the staple strand mix (molar ratio of 10x) in buffer TAE-$MgCl_2$ (40 mM Tris, 20 mM acetic acid, 2 mM EDTA, 16 mM $MgCl_2$, pH 8.0) in a final reaction volume of 50 uL and annealed with the following program: 95°C for 5 min, 80–75°C at 1°C per 5 min, 75–30°C at 1°C per 15 min, and 30–25°C at 1°C per 10 min. In the case of the pentagonal bipyramid, the reverse-complement oligonucleotide to the overhang sequence was added to the reaction mixture at 2-fold excess over the total concentration of the overhang sequence. The folded NPs are stored at 4°C in the folding buffer with the excess of staples strands prior to perform conjugation with antigens.

- **DNA-NP purification**

Before using the DNA-NPs for conjugation with antigens and for the B cell activation assay, the DNA origami objects folded with an excess of staples strands were purified using an Amicon ultra 0.5 centrifugal filter with three washes of folding buffer and an extra wash of 1X PBS for further modification with antigens. In the case of the pentagonal bipyramid, DNA-NPs with overhangs were purified into TAE-$MgCl_2$ buffer prior to functionalization

with antigen and concentrated to at least 5-fold over the target concentration for the functionalization reaction. Centrifugation steps were performed at 1000g for 30–40 minutes and the final concentration of NPs was determined using a NanoDrop 2000. Purified NPs were subsequently modified with antigens or stored in 1X PBS (or TAE-$MgCl_2$ buffer) at 4°C.

- **PNA strand synthesis**

  PNA strands were synthesized in-house using solid phase peptide synthesis. Lysine residues were attached at either end of the PNA sequence to improve solubility. Fmoc-PNA monomers (PNA-Bio, Inc.) were coupled to a low loading Tentagel-S-RAM resin using 4 eq. PNA, 3.95 eq. PyBOP, and 6 eq. diisopropylethylamine (DIEA). Lysine and glycine residues were reacted in the same way. Following each coupling, the peptide was deprotected in 20% piperidine in DMF. N-maleoyl-β-alanine (Sigma) was coupled to the N-terminus under the same coupling conditions. The peptide was then cleaved from the resin in 95% trifluoroacetic acid (TFA), 2.5% H2O, and 2.5% triisopropylsilane. The peptide was dissolved in aqueous solution with 0.1% TFA, filtered, and purified by HPLC using a C-18 Gemini column (Phenomenex) with a mobile phase of acetonitrile containing 0.1% TFA. Purity of the PNA products was analyzed with MALDI-TOF mass spectrometry on a Bruker Daltonics microflex. The sequence of the synthesized PNA strand is: (Maleimide)-GGK-cagtccagt-K-($CONH_2$), and the complementary ssDNA is: 5'-Oligo-TT-ACTGGACTG-3' (melting temperature predicted: 56.7°C). The sequence has been designed to have a melting temperature above 55°C (predicted with the PNA tool: https://www.pnabio.com/support/PNA_Tool.htm, from PNA Bio, Inc.) and orthogonal to the sequence of M13mp18 and validated using NCBI BLAST online tool.

- **Antigen-PNA conjugation**

  PNA strands were conjugated to eOD by reacting the terminal maleimide onto an N-terminal cysteine of eOD. Prior to the reaction, eOD was incubated with a 10-fold molar excess of tris(2-carboxyethyl)phosphine (TCEP) for 15 minutes, after which TCEP was removed using a centrifugal filter. Immediately after removal of TCEP, a 2-fold molar excess of maleimide-PNA was reacted with cysteine-eOD overnight at 4C in PBS. Unreacted PNA was then removed using an Amicon centrifugal filter (10 kDa MWCO).

- **Antigen conjugation with AF647 dye**

  The eOD-PNA conjugate was modified with the fluorescent label AlexaFluor 647-NHS (AF647) using a protocol previously published by Havenar-Daughton et al.[47]. Briefly, eOD-PNA was incubated with 5 molar equivalents of AF647-NHS in 10 mM sodium bicarbonate buffer for 2 hours at room temperature. Unreacted dye was removed using centrifugal filtration (10kDa MWCO).

- **Antigen attachment to DNA-NPs**

  Purified DNA-NPs were mixed with PNA-antigen conjugates at a molar ratio of 5X antigen per overhang on the DNA-NPs in 1X PBS buffer. The concentration of DNA-NPs used was in the range of 50 to 100 nM. An annealing temperature ramp was used for ssPNA-ssDNA

hybridization starting at 37°C and decreasing to 4°C at 1°C per 20 min and kept for at least 4 hours at 4°C prior use for B cell activation assay. Prior to use in the B cell activation assay, modified DNA-NPs were purified using a centrifugal filter, as described in the DNA-NP purification section above, to remove excess free PNA-antigens. Peptide antigens were added from DMF stock solutions and maximal target concentrations of DMF in the functionalization reaction were kept below 5% (v/v). For purification of the functionalized pentagonal bipyramid, centrifugal filters were coated with Pluronic F-127.

- **Structural characterization**

Transmission Electron Microscopy: DNA-NPs were visualized by transmission electron microscopy (TEM) using grids prepared as described previously with minor modifications[48]. Briefly, carbon supported grids with copper mesh (CF200H-CU; Electron Microscopy Sciences) were glow discharged and soaked in 100 μM MgCl2 and blotted prior to depositing DNA-NPs. 20 μl of a 10 nM DNA-NP solution was applied to a clean parafilm surface and the grid was floated for 2 minutes. While soaking, 2% uranyl formate (UF; Electron Microscopy Sciences) was neutralized with 25 mM NaOH final concentration, vortexed for 1 minute, and filtered via syringe through a 0.1 μm filter (EMD Millipore) dropwise onto the clean parafilm surface. The grid was then removed and quickly dried by edge blotting with Whatman 44 ashless paper. The grid was then immediately transferred to the 2% UF solution and incubated for 30 seconds. Again, the grid was dried by blotting along the edge with Whatman paper, and left to dry in air for an additional 30 minutes prior to imaging. Imaging was done on a FEI Tecnai G2 Spirit TWIN set to 120kV equipped with a Gatan camera. Images were acquired at 6,500x for wide-field views and 52,000x for near-field views. Images were collected using 3-second exposures. All raw images were cropped in Adobe Photoshop with subsequent autocontrast applied.

Agarose Gel Electrophoresis: DNA-NPs folded and conjugated with eOD-GT8-PNA were analyzed using agarose gel electrophoresis with 2% agarose gel pre-stained with EtBr. Samples non-purified in folding buffer or purified in PBS buffer were loaded at a concentration of 20 to 50 nM of DNA origami, ran for 2–3 hours at 70 V at 4C and visualized with a transilluminator. For fluorescence gel analysis with the AF647 modified eOD-GT8 images were acquired using a Typhoon FLA 7000 at the SybrSafe excitation wavelength (473 nm), and at the AF647 excitation wavelength (635 nm). Images were subsequently merged using ImageJ software[49].

Fluorescence quantification of DNA-NP coverage with antigen: Quantification of the eOD-GT8 conjugation to DNA-NPs was performed using a Fluoromax-4 (Horiba, Inc.) fluorimeter. eOD-GT8-PNA monomers were modified with AF647 dye using NHS-NH_2 chemistry as described above, prior to conjugation via hybridization to DNA-NPs. eOD-GT8-PNA was incubated with 5 molar equivalents of AF647 for 2 hours, and subsequently purified using centrifugal spin filtration (10k MWCO). The degree of labeling was 2 dyes per protein on average. Spectra were acquired with an excitation wavelength of 630 nm (emission measured at 670 nm). A fluorescence calibration curve was first measured using free monomeric eOD-GT8-PNA conjugated with AF647 dye by varying antigen

concentration, and subsequently used as a reference curve to determine the conjugation yield to DNA-NPs.

Tryptophan assay for quantification of DNA-NP coverage with antigen: A tryptophan fluorescence standard curve (0 to 2 μM) was used to determine the percentage of antigen coverage on DNA-NPs. Tryptophan fluorescence was read on a fluorescence plate reader at 440 nm using an excitation wavelength of 370 nm.

Absorbance quantification of DNA-NP coverage with antigen: For functionalization of purified DNA-NPs with AF-647-labeled peptide antigens, ratiometric absorbance measurements were employed to quantify coverage. The concentration of DNA-NPs was determined via absorbance measurements at 260 nm using a NanoDrop 2000 and compared to the concentration of AF-647 determined at 647 nm (ε = 270,000 1/(cm*M)). Coverage was determined in triplicate and absorbance values were extracted from the same UV-Vis spectrum.

- **B cell Calcium flux assay**

Ramos B Cells at a concentration of 10 million cells/mL were incubated with 10 μM Fluo-4 AM (ThermoFisher, Inc.) for 30 minutes at 37C. After washing once, flux assays were performed on a Tecan plate reader at 37C on a 96 well microplate with 160 μL of Fluo-4 labeled Ramos cells at 2 million cells/mL. A baseline fluorescence was then recorded for 1 minute, and 40 μL of NPs were added to the cells for a final concentration of 5 nM of antigen, unless otherwise stated. A fixed concentration of antigens was used rather than the concentration of DNA-NPs to simplify the comparison between experiments with various DNA-NPs and to assess the role of antigen concentration instead of the role of the DNA-NPs. For studies utilizing the p5 peptide antigen, primary B cells were isolated from 3–83 mouse spleens and stained via the same procedure. Primary B cells were isolated from splenocytes by negative selection using a StemCell EasySep B Cell Isolation Kit.

- **Animals**

Female 3–83 mice (H-2K^{K}-specific BCR) 6–10 weeks of age were used for primary B cell experiments. Mice were handled under local, state, and federal guidelines following an Institutional Animal Care and Use Committee (IACUC)-approved protocol at MIT.

- **B cell Calcium flux data statistical analysis**

Raw calcium traces were normalized to a common baseline by subtracting the PBS timetrace at every timepoint, then dividing the timetrace at every point by the average of the timepoints before antigen addition. The timepoints after antigen addition were then summed for each sample in each repeat to give the calcium release above baseline (I_{tot}). The maximum I_{tot} across all samples within each repeat was determined ($\max(I_{tot})$), and total calcium signaling (Normalized AUC) for each sample within each repeat is then given by $I_{tot} / \max(I_{tot})$. Repeats were averaged together to yield the bar height for graphs in Figures 2–4. Student's t-test was performed on the Normalized AUCs entering into this average, where in most cases N=3 replicates.

- **B cell imaging**

Sample preparation for confocal microscopy: Ramos cells were labeled on ice at a concentration of 5 million/mL and protected from light for 30 minutes in Hank's Buffered Salt Solution (HBSS) with 20 μg/mL human anti IgM f(Ab)1 fragment (Jackson 109-007-043) conjugated to Janelia Fluor 549. Cells were spun down and resuspended in warm HBSS at a concentration of 2 million/mL. Antigens were added to a final concentration of 5 nM by adding 50 μL antigen solution to a volume of cells between 175 μL and 400 μL, and cells were kept at 37C by incubation in a thermal bead bath. At timepoints following the addition of antigen, 100 μL of cells were removed and placed into 200 μL of 6% warm PFA solution and allowed to fix for 10 minutes at 37C. Following fixation, fixed cells were permeabilized by HBSS containing 0.1% triton-X and washed before to be diluted in 4.5 mL HBSS and centrifuged at 600g for 5 minutes. Cells were then labeled for 5 hours at 4C in 50 μL HBSS with a 1:100 dilution of anti-phospho Syk primary Ab (Millipore Sigma) and a 1:50 dilution of Phalloidin conjugated to Alexa 405 in the presence of 5 mg/mL bovine serum albumin (BSA, Sigma) and 0.1% Triton-X. Cells were diluted into 4.5 mL HBSS and centrifuged at 600g for 5 minutes, and resuspended in 4.5 mL HBSS and centrifuged again to wash before being resuspended in 100 μL HBSS. Cells were then labeled with a 1:100 dilution of secondary anti-rabbit conjugated to AF488 for 1 hour at 4C in the presence of 5 mg/ml BSA and 0.1% Triton-X, before being washed twice as above. Cells were then plated onto LabTech II 8-well glass bottom chambers modified with 0.1% Poly-L-Lysine (PLL, Sigma P8920) and allowed to adhere for at least 4 hours at 4C before performing confocal microscopy.

Confocal Microscopy imaging: Confocal microscopy was performed on a Zeiss AxioVert 200M inverted microscope stand with Yokogawa CSU-22 spinning disk confocal scan head with Andor Borealis multi-point confocal system. Probes were excited by 4 laser lines in the Andor / Spectral applied Research Integrated Laser Engine: 405 nm 100 mW OPSL, 488 nm 150 mW OPSL, 561 nm 100 mW OPSL, and 642 nm 110 mW OPSL. Multipass dichroic mirror 405/488/568/647 and emission filters 450/50 nm, 525/50 nm, 605/70 nm, and 700/75 nm were used for each emission channel, respectively. Sample was imaged through a 63x oil Plan Apochromat objective with an effective pixel size of 0.092 μm/pixel. Images were captured through a Hamamatsu Orca-ER cooled CCD, and instrumentation was controlled through MetaMorph software. For each image, 9 z-planes having separation of 1.5 μm were acquired between the top and bottom of the cell, and approximately 10 fields of view were acquired for each sample.

Image analysis: 16-bit images were read into MATLAB and converted to double precision. For each field of view, a maximum intensity projection (MIP) was calculated for the phalloidin channel. This was then binarized using adaptive thresholding, cleaned of stray pixels, and then morphological opening and closing was performed. Holes within this binarization were then filled, and discreet objects within this binarization were labeled as individual cells. For each cell in a field of view, z-planes were binarized as above using the phalloidin channel, and these z-plane binarizations were restricted to the limit of the MIP binarization for each cell. The convex hull of this z-plane binarization was used to estimate the extent of the cell, and the cell surface was estimated by selecting the perimeter of the z-

plane binarization and dilating this 25 times in a 4-connected neighborhood and subsequent restriction by the undilated cell extent binarization. The total intensity of cellular probes and the surface intensity of cellular probes was calculated through summation using all z-stacks after logical indexing of the background-subtracted raw z-plane images, where background was estimated to be a constant through all z-planes and channels. Pixel-based correlation was performed through pairwise linear correlation of pixel values between channels following logical indexing. Average intensity values shown are an average over cells, and errorbars shown are the standard errors of the means, given by the standard deviation divided by sqrt(N_{cells}). Internalized fraction of probe intensity for a single cell is given by (total cell intensity – cell surface intensity) / total cell intensity.

Supplementary Material

Refer to Web version on PubMed Central for supplementary material.

Acknowledgements

This work was supported by the Human Frontier Science Program (RGP0029/2014), the Office of Naval Research (N00014-16-1-2953), the U. S. Army Research Office through the Institute for Soldier Nanotechnologies at MIT (Cooperative Agreement Number W911NF-18-2-0048), the Ragon Institute of MGH, MIT, and Harvard, and the NIH (R21-EB026008, R01-MH112694, AI048240, UM1AI144462, and UM1AI100663). W.R.S. acknowledges funding from funding by the IAVI Neutralizing Antibody Consortium (NAC) and Center, and the Collaboration for AIDS Vaccine Discovery funding for the IAVI NAC Center. J.D. is supported by the NIH (R01-AI 143740, R01-AI 146581). E.-C. W. is supported by the Feodor Lynen Fellowship of the Alexander von Humboldt Foundation. DJI is an investigator of the Howard Hughes Medical Institute.

References

1. Bachmann MF & Jennings GT Vaccine delivery: a matter of size, geometry, kinetics and molecular patterns. Nat. Rev. Immunol 10, 787–796 (2010). [PubMed: 20948547]
2. Puffer EB, Pontrello JK, Hollenbeck JJ, Kink JA & Kiessling LL Activating B cell signaling with defined multivalent ligands. ACS Chem. Biol 2, 252–262 (2007). [PubMed: 17432821]
3. Minguet S, Dopfer E-P & Schamel WWA Low-valency, but not monovalent, antigens trigger the B-cell antigen receptor (BCR). Int. Immunol 22, 205–212 (2010). [PubMed: 20145007]
4. Batista FD, Iber D & Neuberger MS B cells acquire antigen from target cells after synapse formation. Nature 411, 489 (2001). [PubMed: 11373683]
5. Dintzis HM, Dintzis RZ & Vogelstein B Molecular determinants of immunogenicity: the immunon model of immune response. Proc. Natl. Acad. Sci. U. S. A 73, 3671–3675 (1976). [PubMed: 62364]
6. Brouwer PJM et al. Enhancing and shaping the immunogenicity of native-like HIV-1 envelope trimers with a two-component protein nanoparticle. Nat. Commun 10, 1–17 (2019). [PubMed: 30602773]
7. Steichen JM et al. HIV Vaccine Design to Target Germline Precursors of Glycan-Dependent Broadly Neutralizing Antibodies. Immunity 45, 483–496 (2016). [PubMed: 27617678]
8. Abbott RK et al. Precursor Frequency and Affinity Determine B Cell Competitive Fitness in Germinal Centers, Tested with Germline-Targeting HIV Vaccine Immunogens. Immunity 48, 133–146.e6 (2018). [PubMed: 29287996]
9. Stamatatos L, Pancera M & McGuire AT Germline-targeting immunogens. Immunol. Rev 275, 203–216 (2017). [PubMed: 28133796]
10. Steichen JM et al. A generalized HIV vaccine design strategy for priming of broadly neutralizing antibody responses. Science 366, (2019).
11. Saunders KO et al. Targeted selection of HIV-specific antibody mutations by engineering B cell maturation. Science 366, (2019).

12. Jardine JG et al. HIV-1 VACCINES. Priming a broadly neutralizing antibody response to HIV-1 using a germline-targeting immunogen. Science 349, 156–161 (2015). [PubMed: 26089355]
13. Sok D et al. Priming HIV-1 broadly neutralizing antibody precursors in human Ig loci transgenic mice. Science 353, 1557–1560 (2016). [PubMed: 27608668]
14. Kim Y-M et al. Monovalent ligation of the B cell receptor induces receptor activation but fails to promote antigen presentation. Proc. Natl. Acad. Sci. U. S. A 103, 3327–3332 (2006). [PubMed: 16492756]
15. Bennett NR, Zwick DB, Courtney AH & Kiessling LL Multivalent Antigens for Promoting B and T Cell Activation. ACS Chem. Biol 10, 1817–1824 (2015). [PubMed: 25970017]
16. Bachmann MF et al. The influence of antigen organization on B cell responsiveness. Science 262, 1448–1451 (1993). [PubMed: 8248784]
17. Rothemund PWK Folding DNA to create nanoscale shapes and patterns. Nature 440, 297–302 (2006). [PubMed: 16541064]
18. Veneziano R et al. Designer nanoscale DNA assemblies programmed from the top down. Science 352, 1534–1534 (2016). [PubMed: 27229143]
19. Wamhoff E-C et al. Programming Structured DNA Assemblies to Probe Biophysical Processes. Annu. Rev. Biophys 48, 395–419 (2019). [PubMed: 31084582]
20. Jardine JG et al. HIV-1 broadly neutralizing antibody precursor B cells revealed by germline-targeting immunogen. Science 351, 1458–1463 (2016). [PubMed: 27013733]
21. Jardine J et al. Rational HIV immunogen design to target specific germline B cell receptors. Science 340, 711–716 (2013). [PubMed: 23539181]
22. Havenar-Daughton C et al. The human naive B cell repertoire contains distinct subclasses for a germline-targeting HIV-1 vaccine immunogen. Sci. Transl. Med 10, eaat0381 (2018). [PubMed: 29973404]
23. Schwarz FP, Robinson S & Butler JM Thermodynamic comparison of PNA/DNA and DNA/DNA hybridization reactions at ambient temperature. Nucleic Acids Res. 27, 4792–4800 (1999). [PubMed: 10572180]
24. Scharenberg AM, Humphries LA & Rawlings DJ Calcium signalling and cell-fate choice in B cells. Nat. Rev. Immunol 7, 778–789 (2007). [PubMed: 17853903]
25. Sil D, Lee JB, Luo D, Holowka D & Baird B Trivalent Ligands with Rigid DNA Spacers Reveal Structural Requirements For IgE Receptor Signaling in RBL Mast Cells. ACS Chem. Biol 2, 674–684 (2007). [PubMed: 18041817]
26. Cochran JR, Cameron TO, Stone JD, Lubetsky JB & Stern LJ Receptor Proximity, Not Intermolecular Orientation, Is Critical for Triggering T-cell Activation. J. Biol. Chem 276, 28068–28074 (2001). [PubMed: 11384988]
27. Yang J & Reth M Oligomeric organization of the B-cell antigen receptor on resting cells. Nature 467, 465–469 (2010). [PubMed: 20818374]
28. Liu W, Wang H & Xu C Antigen Receptor Nanoclusters: Small Units with Big Functions. Trends Immunol. 37, 680–689 (2016). [PubMed: 27555115]
29. Gold MR & Reth MG Antigen Receptor Function in the Context of the Nanoscale Organization of the B Cell Membrane. Annu. Rev. Immunol 37, 97–123 (2019). [PubMed: 31026412]
30. Tolar P & Pierce SK A Conformation-Induced Oligomerization Model for B cell Receptor Microclustering and Signaling in Immunological Synapse (eds. Saito T & Batista FD) vol. 340 155–169 (Springer Berlin Heidelberg, 2010).
31. Shaw A et al. Binding to nanopatterned antigens is dominated by the spatial tolerance of antibodies. Nat. Nanotechnol 14, 184 (2019). [PubMed: 30643273]
32. Kouskoff V et al. Antigens Varying in Affinity for the B Cell Receptor Induce Differential B Lymphocyte Responses. J. Exp. Med 188, 1453–1464 (1998). [PubMed: 9782122]
33. Harwood NE & Batista FD Early events in B cell activation. Annu. Rev. Immunol 28, 185–210 (2010). [PubMed: 20192804]
34. Stone MB, Shelby SA, Núñez MF, Wisser K & Veatch SL Protein sorting by lipid phase-like domains supports emergent signaling function in B lymphocyte plasma membranes. eLife 6, e19891 (2017). [PubMed: 28145867]

35. Tolar P Cytoskeletal control of B cell responses to antigens. Nat. Rev. Immunol 17, 621–634 (2017). [PubMed: 28690317]
36. Mukherjee S et al. Monovalent and Multivalent Ligation of the B Cell Receptor Exhibit Differential Dependence upon Syk and Src Family Kinases. Sci. Signal 6, ra1 (2013). [PubMed: 23281368]
37. Kläsener K, Maity PC, Hobeika E, Yang J & Reth M B cell activation involves nanoscale receptor reorganizations and inside-out signaling by Syk. eLife 3, e02069 (2014). [PubMed: 24963139]
38. Tolar P, Hanna J, Krueger PD & Pierce SK The constant region of the membrane immunoglobulin mediates B cell-receptor clustering and signaling in response to membrane antigens. Immunity 30, 44–55 (2009). [PubMed: 19135393]
39. Lee J, Sengupta P, Brzostowski J, Lippincott-Schwartz J & Pierce SK The nanoscale spatial organization of B-cell receptors on immunoglobulin M- and G-expressing human B-cells. Mol. Biol. Cell 28, 511–523 (2017). [PubMed: 27974642]
40. Liu W, Meckel T, Tolar P, Sohn HW & Pierce SK Antigen affinity discrimination is an intrinsic function of the B cell receptor. J. Exp. Med 207, 1095–1111 (2010). [PubMed: 20404102]
41. Zhu P et al. Distribution and three-dimensional structure of AIDS virus envelope spikes. Nature 441, 847 (2006). [PubMed: 16728975]
42. Marcandalli J et al. Induction of Potent Neutralizing Antibody Responses by a Designed Protein Nanoparticle Vaccine for Respiratory Syncytial Virus. Cell 176, 1420–1431.e17 (2019). [PubMed: 30849373]
43. Weaver GC et al. In vitro reconstitution of B cell receptor-antigen interactions to evaluate potential vaccine candidates. Nat. Protoc 11, 193–213 (2016). [PubMed: 26741406]
44. Villar RF et al. Reconstituted B cell receptor signaling reveals carbohydrate-dependent mode of activation. Sci. Rep 6, 1–11 (2016). [PubMed: 28442746]
45. Veneziano R et al. In vitro synthesis of gene-length single-stranded DNA. Sci. Rep 8, (2018).
46. Shepherd TR, Du RR, Huang H, Wamhoff E-C & Bathe M Bioproduction of pure, kilobase-scale single-stranded DNA. Sci. Rep 9, 6121 (2019). [PubMed: 30992517]
47. Havenar-Daughton C et al. Rapid Germinal Center and Antibody Responses in Non-human Primates after a Single Nanoparticle Vaccine Immunization. Cell Rep. 29, 1756–1766.e8 (2019). [PubMed: 31722194]
48. Marras AE, Zhou L, Su H-J & Castro CE Programmable motion of DNA origami mechanisms. Proc. Natl. Acad. Sci 112, 713–718 (2015). [PubMed: 25561550]
49. Schneider CA, Rasband WS & Eliceiri KW NIH Image to ImageJ: 25 years of image analysis. Nat. Methods 9, 671–675 (2012). [PubMed: 22930834]

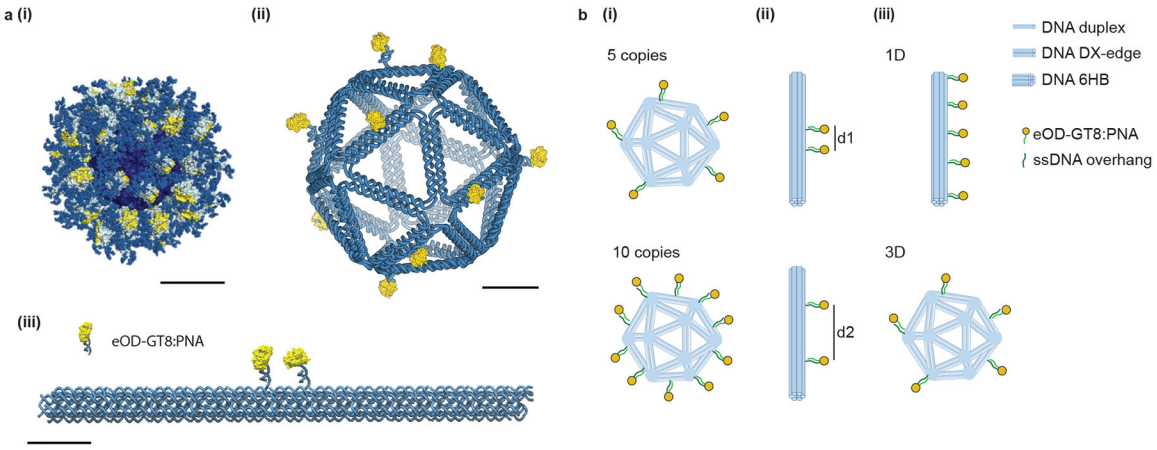

Fig. 1. Scaffolded DNA origami nanoparticles to control nanoscale organization of HIV immunogens.

(a) DNA-NPs were designed to self-assemble the eOD-GT8 antigen in a controlled manner, mimicking features of the eOD-GT8–60mer immunogen. (**i**) eOD-GT8–60mer protein NP; (**ii**) Icosahedral DNA-NP presenting 10 copies of eOD-GT8 (Ico-10x); and (**iii**) 6HB rod-like structure presenting two copies of eOD-GT8 (6HB-2x). Scale bars are 10 nm. **(b)** Both the icosahedral and 6HB structures were used to explore the **(i)** stoichiometry; **(ii)** inter-antigen distance, d1 and d2; and **(iii)** 1D versus 3D dimensionality of eOD-GT8 antigens presentation (DX: double-crossover).

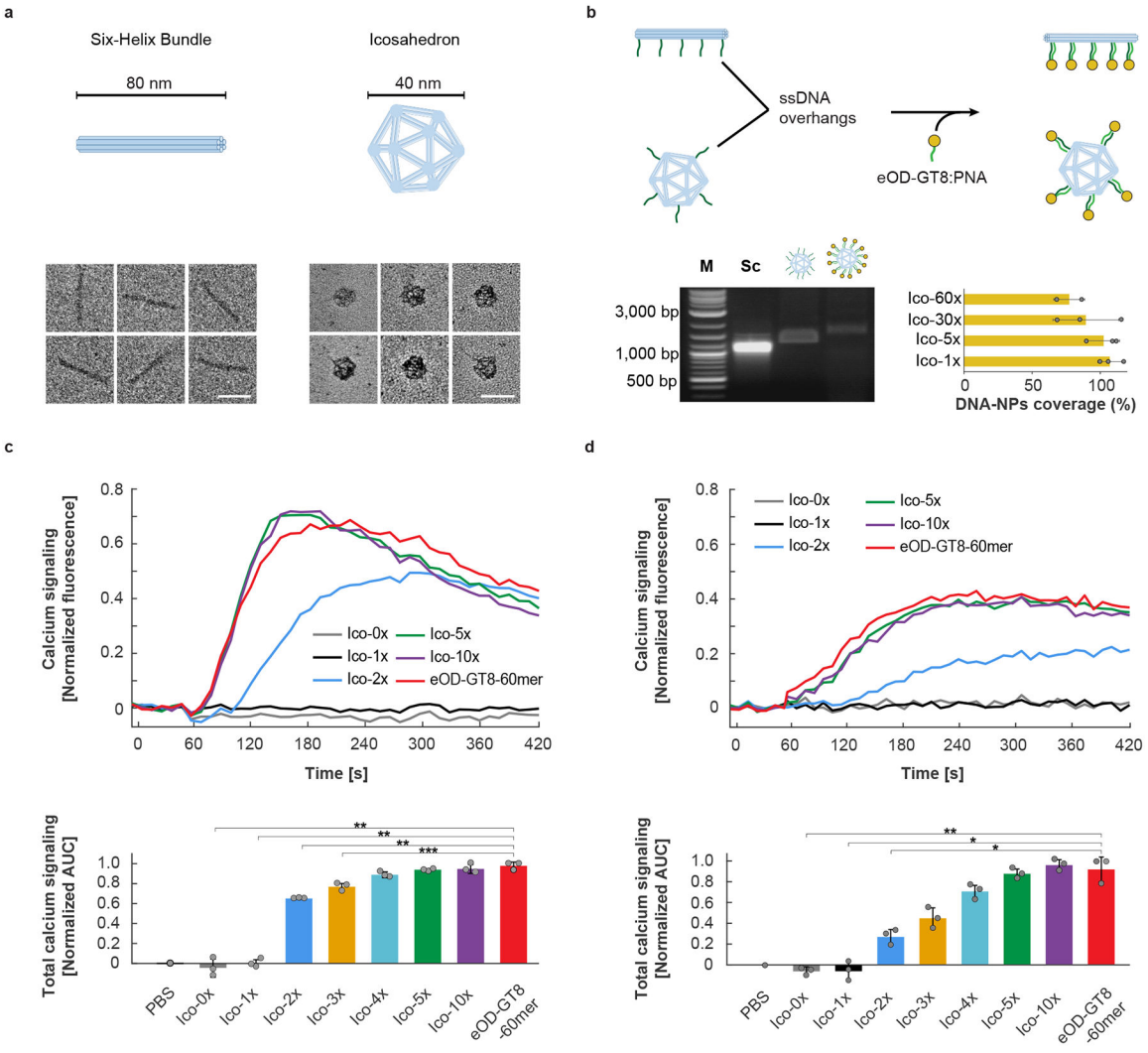

Fig. 2. Increasing antigen valency improves B cell responses to nanoparticle antigens up to a threshold.

(a) Folding of the two types of DNA-NPs (six-helix bundle, 6HB, and DNA icosahedron) that were designed and used in this study for 1D versus 3D presentation of antigens. TEM images show high folding yield and monodisperse DNA-NPs. (Scale bar: 40 nm) **(b)** Overview of the antigen conjugation protocol to attach eOD-GT8 antigens to the DNA-NPs using PNA single strands complementary to ssDNA overhangs on the DNA-NPs and characterization with electrophoresis. Shown are representative gel electrophoresis samples and fluorescence quantification of four different icosahedral DNA-NPs conjugated with eOD-GT8:PNA-AF647 (Ico-1x; Ico-5x; Ico-30x; Ico-60x)); (M, Molecular weight Marker; Sc, Scaffold; bp: base pair). Error bars represent standard deviation of the mean (n=3 biological replicates/group for fluorescence quantification). **(c** and **d)** DNA-NPs modified with eOD-GT8 activate IgM-BCR at both **(c)** 5 nM and **(d)** 0.5 nM eOD-GT8. Fluo-4 calcium probe fluorescence is shown in the top row (representative individual calcium traces), and average area-under-the-curve measurements for calcium signaling normalized to the maximum response of all samples in a repeat are shown in the bottom row. For (**c**) and

(**d**) Error bars represent standard deviation of the mean (n=3 biological replicates/group). P-values are from a two-way ANOVA, paired Student's t-test (*: $p<0.05$; **: $p<0.01$; ***: $p<0.001$. All P-values are available in the Supplementary Table 5). (The electron microscopy images in **a** are from 3 technical replicates [10 images per replicates] with similar results. The gels in **b** have been repeated 3 times (biological replicates) with similar results).

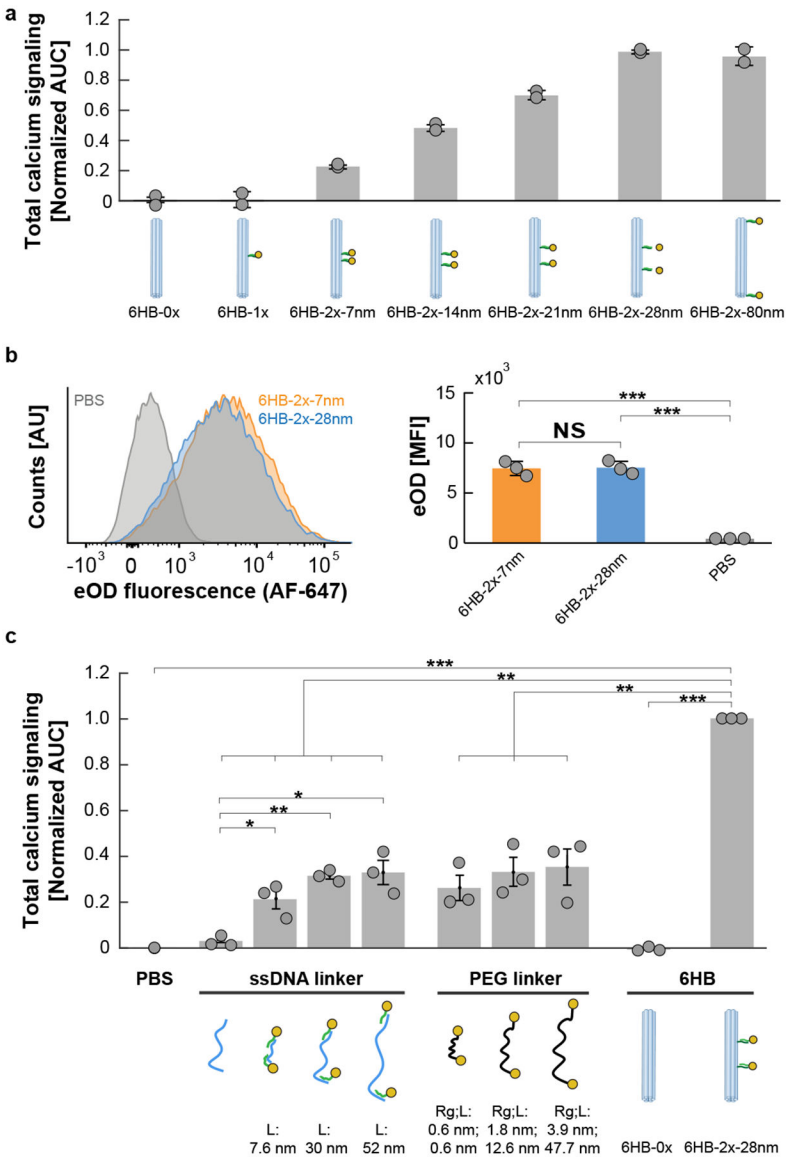

Fig. 3. IgM-BCR response increases and then plateaus with increasing inter-antigen distance on a rigid scaffold.

(a) Area-under-the-curve total calcium signaling in glVRC01 B cells stimulated with DNA-NP eOD-GT8 dimers with inter-antigen distances between 7 nm and 80 nm at an antigen concentration of 5 nM (n=2 biological replicates/group). Fluo-4 AUC is normalized as in Figure 2, where error bars represent standard deviations of the mean. **(b)** Representative flow cytometry plots of 6H-2x-7nm, and 6HB-2x-28nm binding to antigen-specific B cells (left) after 30 min incubation at 4°C at a fixed antigen concentration of 5 nM. (Right) Quantitation of data from flow cytometry (MFI: Mean Fluorescence Intensity, (n=3 distinct biological replicates/group), where error bars represent standard deviations of the mean and the P-values are from a one-way ANOVA, followed by Tukey post hoc comparison test (***: $p<0.001$; NS: Not statistically significant, $p=0.9999$. All P-values are available in the Supplementary Table 6). **(c)** Total calcium release (Fluo-4 fluorescence) integrated over 7 minutes following antigen addition from cells stimulated with eOD-GT8 dimers attached to

the flexible polymeric scaffolds (ssDNA or PEG), compared with rigid 6HB DNA-NP eOD-GT8 dimer structures at a fixed antigen concentration of 5 nM (n=3 distinct biological replicates/group). Fluo-4 AUC is normalized as in Figure 2, where error bars represent standard deviations of the mean and P-values are from a two-way ANOVA, paired Student's t-test (*: $p<0.05$; **: $p<0.01$; ***: $p<0.001$. All P-values are available in the Supplementary Table 7). (L: Contour Length; Rg: Radius-of-Gyration).

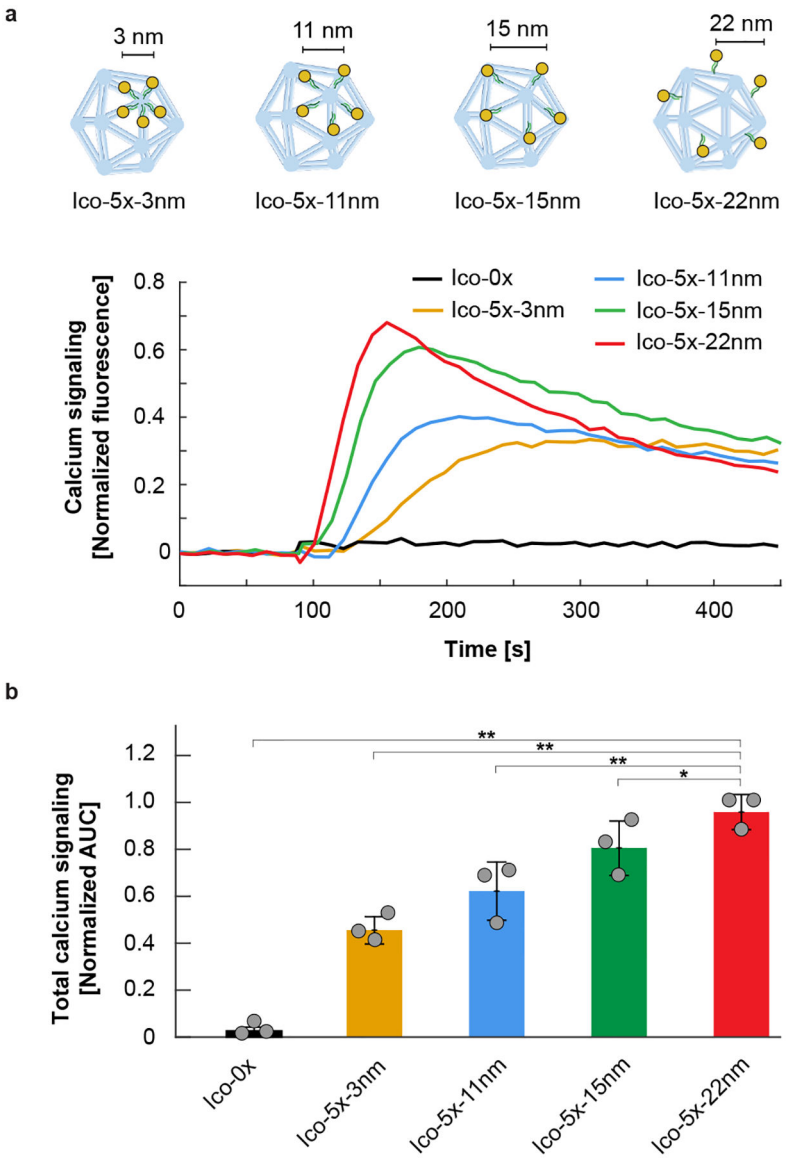

Fig. 4. Clustering of antigens on one face of an icosahedral DNA-nanoparticle.

(a) Fluo-4 calcium probe fluorescence versus time following addition of 5 nM eOD-GT8 antigen to glVRC01 B cells. Icosahedral (Ico) structures with varying inter-antigen distances are plotted in the same graph. (Representative individual calcium traces, n=3 biological replicates with similar results) (**b)** Total calcium signaling integrated over 6 min following antigen addition from cells stimulated with different Ico-5x structures presenting antigen at a total concentration of 5 nM eOD-GT8 (n=3 biological replicates/group). Fluo-4 AUC is normalized as in Figure 2, where error bars represent standard deviations of the mean and P-values are from a two-way ANOVA, paired Student's t-test (*: $p<0.05$; **: $p<0.01$. All P-values are available in the Supplementary Table 8).

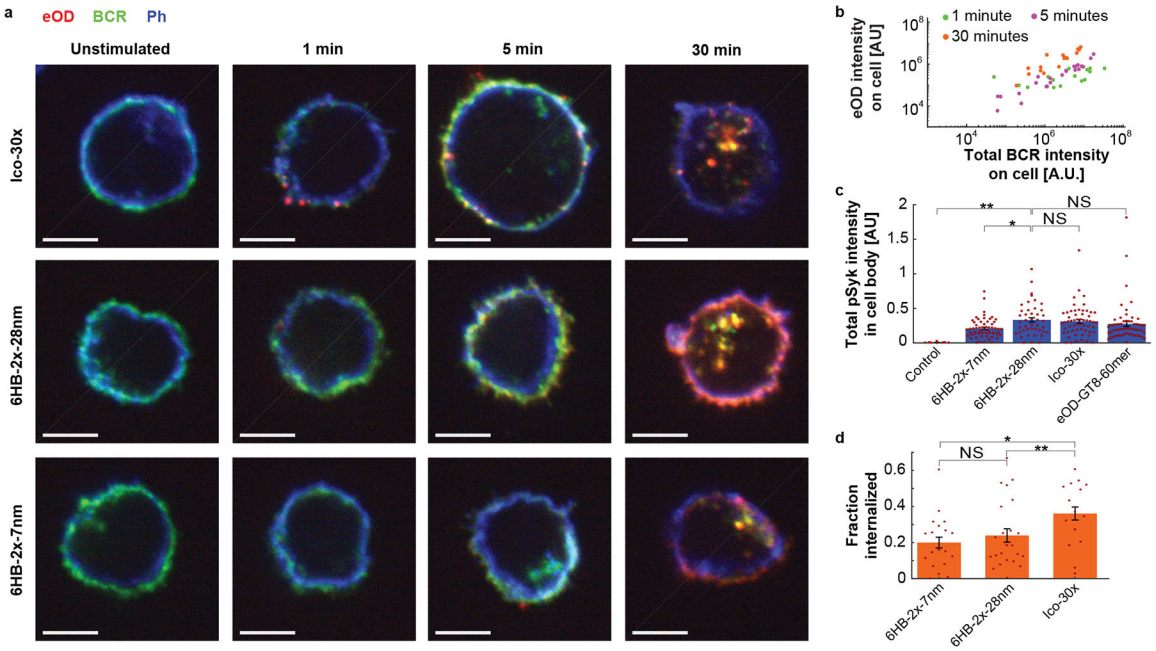

Fig. 5. Confocal microscopic imaging of DNA-nanoparticles on Ramos B cells.

(a) Time series imaging of Ico-30x, 6HB-2x-28nm, and 6HB-2x-7nm shows surface binding and internalization into Ramos B-cells. Here, eOD-GT8 was fluorescently labelled with Alexa Fluor 647, VRC01 IgM-BCR was labeled with a FAb fragment conjugated to Janelia Fluor 549 prior to antigen addition, and actin was labeled with phalloidin Alexa Fluor 405 after cell fixation. Scale bar is 5 μm. This experiment has been performed twice (n=2 biological replicates) with similar results. **(b)** Total intensity of eOD-GT8 is highly correlated with intensity of IgM-BCR, confirming specific binding of NPs to the IgM-BCR and co-internalization. Numbers of cells analyzed are 15 (1 min), 23 (5 min), 16 (30 min), cells are from the same culture. **(c)** Ramos cells were labeled with an anti-phospho-Syk antibody after fixation and the total pSyk intensity per cell was determined. Numbers of cells analyzed are 11 (control), 58 (6HB-2x-7nm), 43 (6HB-2x-28nm), 56 (Ico-30x), and 56 (eOD-GT8–60mer), cells are from the same culture. **(d)** Internalized fraction of eOD was estimated by segmenting the cell surface using a phalloidin stain as detailed in Methods. Total internal eOD fluorescence was divided by total cellular eOD fluorescence on a cell-by-cell basis. Numbers of cells analyzed are 19 (6HB-2x-7nm), 23 (6HB-2x-28nm), and 15 (Ico-30x), cells are from the same culture. In (**c**) in (**d**), error bars denote the standard error of the mean fluorescence between cells with significance determined by a two-sided Student's t-test (*: p=0.0314; **: p=0.0016;; NS: Not statistically significant, p= 0.3038 for 6HB-2x-28nm/Ico-30x, and p= 0.4153 for 6HB-2x-28nm/eOD-GT8–60mer). In (**d**), error bars denote the standard error of the mean fluorescence between cells with significance determined by Student's t-test (*: p=0.0142; **: p=0.0074; NS: Not statistically significant, p=0.55). (All P-values are available in the Supplementary Table 9)